Chapter 1

Ultrafast cluster electron and Coulomb explosion dynamics driven by ultraintense laser fields

Isidore Last, Andreas Heidenreich, and Joshua Jortner

School of Chemistry, Tel Aviv University, 69978 Tel Aviv, Israel

1. Prologue

Ultraintense table top lasers are characterized by a maximal intensity of $\sim 10^{20}$ Wcm^{-2}, which constitutes the highest light intensity on earth. Novel features of light-matter interactions emerge from the interaction of clusters with ultrashort (pulse temporal width τ = 10-100 fs) and ultraintense (peak intensity $I_M = 10^{15}$-10^{20} Wcm^{-2}) laser fields [1-14]. The modern research area of femtosecond cluster dynamics on the time scale of nuclear motion is transcended by moving towards attosecond-femtosecond electron dynamics in ultraintense laser fields. The response of clusters to ultraintense lasers induces well characterized ultrafast dynamics of electrons (on time scales of ~ 1-100fs) and of ions (on time scales of 5-100 fs) in these large finite systems [5-14].

We shall address some of the novel physical features of the response and dynamics of homonuclear and heteronuclear clusters in ultraintense laser fields, which pertain to:

(1) New mechanisms of cluster extreme multielectron ionization.

(2) The consequences of the interaction of an ultraintense laser with a spatially confined cluster. A cluster of n constituents (each with m atomic constituents) initially results in confined mn ions of extremely high charges, as well as bare nuclei, e.g., H^+, D^+, C^{4+}, C^{6+}, O^{6+}, O^{8+}, Xe^{q+} (q = 8-36), I^{q+} (q = 7-35) [1-14].

(3) The implications of Coulomb instability of highly multicharged clusters. These result in the interplay between cluster fission [15,16], i.e., instability towards cluster dissociation into two (or a small number

of) large ionic fragments and cluster Coulomb explosion (CE) [16,17] into a large number of small ionic species (Fig. 1).

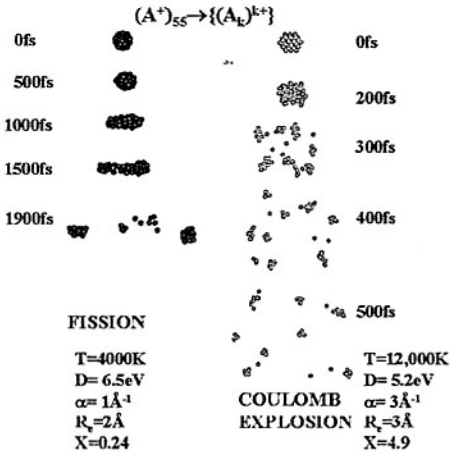

Fig. 1. Molecular dynamics snapshots of fragmentation of highly charged $(A^+)_{55}$ Morse clusters (adopted from data of ref. 16). The potential parmeters were varied, changing the fissibility parameter X = E(Coulomb)/ 2E(surface). Note fission for X < 1 and CE for X > 1.

(4) The formation of high-energy, highly charged ions and bare nuclei, in the energy domain of nuclear physics (1keV – 1meV) via cluster CE [2-4,6-14].

(5) New effects of boosting of the energy by energetic driving and kinematic runover effects of the light ions (e.g., D^+) by highly charged heavy ions, e.g., C^{q+} (q = 4,6) or I^{q+} (q = 7-35), in the CE of heteroclusters [8-12].

(6) The dramatic effects of nuclear fusion driven by cluster CE [1-4,9-14].

2. Extreme Cluster Multielectron Ionization

The ionization of a single q-fold charged atomic or molecular ion with an ionization potential P_q in a laser electric field F_ℓ, whose peak is $|F_\ell^M| = 2.745 \times 10^{-7} (I_M/Wcm^{-2})^{1/2}$ $(eV Å^{-1})$ can be described in terms of the barrier suppression ionization (BSI) mechanism [6], which (in the absence of electron tunneling effects) results in the threshold field for inducing classical ionization is $|eF| = P_q^2 / 4\bar{B}(k+1)$, where $F = F_\ell$ and $\bar{B} = 14.4eV$. The BSI model predictions [6] for multielectron ionization of Xe atoms estimated with $F = F_\ell^M$ are in accord with experiment (Fig. 2) in the range $I_M = 10^{16}$–10^{18} Wcm^{-2}, where highly charged Xe^{q+} (q = 8–16) single ions are produced.

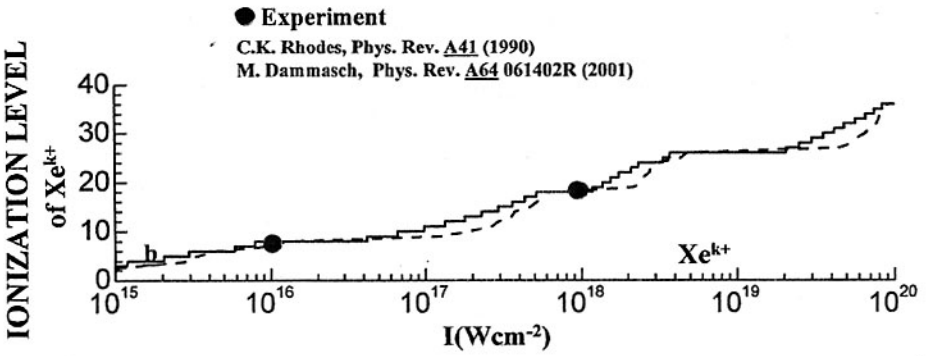

Fig. 2. The laser peak intensity dependence of the ionization level of a single Xe atom [6]. BSI (solid line) and ADK model (dashed line). The dots represent experimental data [6].

Extreme cluster multielectron ionization in ultraintense laser fields (involving the stripping of all electrons from light, first row atoms and the formation of heavily charged ions, e.g., Xe^{26+} or I^{25+} at $I_M = 10^{19}$ Wcm^{-2}) is distinct, both from the electron dynamic response in ordinary fields ($I_M \leq 10^{13}$ Wcm^{-2}), where perturbative quantum electrodynamics is applicable, and from the response of a single atomic or molecular species in terms of mechanisms, the ionization level and time scales for electron and nuclear dynamics. On the basis of our recent analyses and simulations [6-14,18], the electron dynamics of elementary and molecular clusters, e.g., $(Xe)_n$, $(D_2)_n$, $(CD_4)_n$, $(AI)_n$, $(CA_3I)_n$ (with A = H, D or T), in ultraintense laser fields involves three sequential–parallel processes of inner ionization, the nanoplasma formation, and outer ionization [6-9].

The laser electric field acting on the elemental or molecular cluster is taken as $F_\ell(t) = F_{\ell 0}(t)\cos(2\pi\nu t)$, where ν is the laser frequency and $F_{\ell 0}(t)$ is the pulse envelope function. Molecular dynamics simulations (including magnetic field and relativistic effects) [6-9,14] and analyses of high-energy electron dynamics and nuclear dynamics in a cluster interacting with a Gaussian laser field $F_{\ell 0}(t) = F_\ell^M \exp[-2.773(t/\tau)^2]$, with $\nu = 0.35$ fs^{-1} (photon energy 1.44eV and pulse temporal width (FWHM) $\tau = 25$fs), elucidated the time dependence of inner ionization, the formation, persistence and decay of the nanoplasma and of outer ionization.

The cluster inner ionization [5,6,18] is driven by two processes: (A) The BSI mechanism, which is induced by a composite field $\mathbb{F} = \mathbb{F}_\ell + \mathbb{F}_i$, where $\mathbb{F}_i$ is the innter field generated by electrostatic interactions with the ions (ignition effects) and with the nanoplasma electrons (screening effects). The BSI level and time-resolved dynamics were evaluated from the expression for

the threshold field F given above [6]. (B) Electron impact ionization (EII), which involved inelastic, reactive impact ionization of ions by the nanoplasma electrons [5,6,18]. EII in Xe_n clusters was explored using experimental data for the energy dependence of ionization cross sections of Xe^{j+} ions (j = 1–10), which were fit by a three-parameter Lotz-type equation [18]. The relative yields of EII are lower than those for BSI, increasing with increasing the cluster radius R_0 at fixed I_M, and decreases with increasing I_M at fixed R_0 (and n). For Xe_{1061} at $I_M = 10^{15}$ Wcm^{-2}, the ratio of the yields for EII and for BSI (at $\tau = 25fs$) is ~50% [18]. The relative EII yield increases markedly with increasing τ, opening avenues for the control of the ionization level [18].

The ionization level of Xe_n clusters (characterized by the average charge $q_{av} = \langle q \rangle$ on each ion), which manifests the production of $\{Xe^{q+}\}_n$ multicharged ions is presented in Fig. 3, where we also portray the ionization levels of a single Xe atom at each intensity (marked by horizontal arrows). In the highest intensity domain of $I_M = 10^{19}$–10^{20} Wcm^{-2}, q_{av} = 26–36 per ion is very large, being independent of the cluster size. For $I_M = 10^{18}$ Wcm^{-2}, q_{av} increases with increasing R_0, manifesting ignition effects. For $I_M = 10^{17}$ Wcm^{-2}, q_{av} first increases and then decreases with increasing R_0, exhibiting the interplay between ignition effects and nanoplasma screening effects. For $I_M = 10^{17}$–10^{20} Wcm^{-2}, the q_{av} for the clusters converges to the single atom ionization level with decreasing R_0. For $I_M = 10^{15}$ Wcm^{-2}, q_{av} for small clusters is considerably larger than the single atom ionization level, due to the contribution of inner field effects and EII. These results unveil new features of cluster multielectron ionization, which gives rise to a large number (n) of highly charged atoms or nuclei (e.g., up to Xe^{36+}, I^{35+}, C^{6+}, O^{8+}) for novel chemical and physical applications.

Simulation results [7] for electron dynamics (for $\tau = 25fs$), which are expressed in terms of the number of electrons depleted per constituent atom, i.e., n_{ii} (n_{oi}) for inner (outer) ionization (Figs. 4 and 5), exhibit a gradual rise and long-time saturation. The characteristic times for inner/outer ionization of Xe_n (n = 479,1061) clusters are (7–30fs)/(5–13fs) and decrease with increasing I_M. Quasi-resonance effects in the nanoplasma are manifested in the temporal oscillations of the n_{oi} and in the center of gravity of the nanoplasma electrons (Fig. 4 and 5), driving outer ionization.

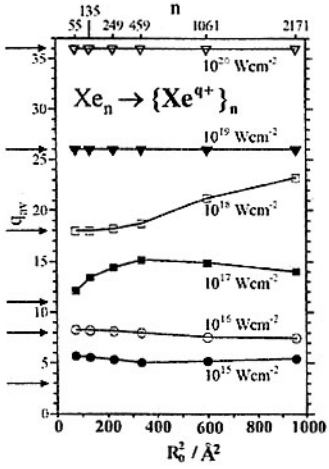

Fig. 3. Cluster size and laser intensity (marked on the curves) dependence of the average inner ionization level of each atom for Xe_n clusters (τ = 25fs). The ionization levels of a single atom are marked by horizontal arrows.

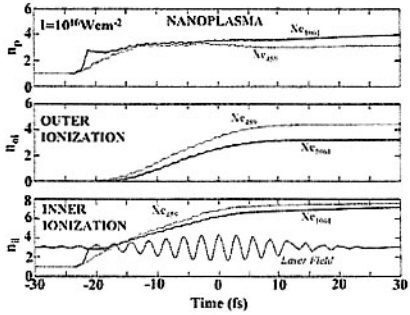

Fig. 4. Time-resolved electron dynamics in Xe_n (n = 1061,459) clusters driven by a Gaussian laser field with $I_M = 10^{16}$ Wcm^{-2} (represented on arbitrary scale in the lower panel). The numbers of electrons n_{ii}, n_{oi} and n_P per atom (see text) are presented.

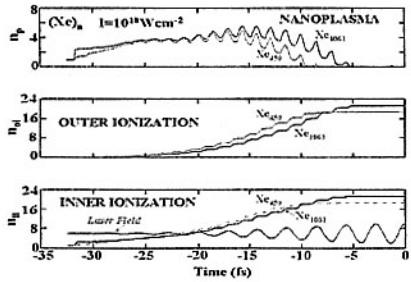

Fig. 5. Same as for Figure 2 with $I_M = 10^{18}$ Wcm^{-2}.

3. The Nanoplasma

The nanoplasma is formed from the unbound electrons generated by inner ionization, which are confined to the cluster and to its vicinity, and by the cluster ions. The number of electrons in the nanoplasma (per atomic constituent) is $n_p = n_{ii}-n_{oi}$. n_p first increases and subsequently either reaches saturation for lower intensities $I_M = 10^{16}$ Wcm^{-2} (Fig. 4) or is completely depleted at $I_M = 10^{18}$ Wcm^{-2} (Fig. 5). The spatial structure and response of the nanoplasma (Figs. 6 and 7) reveals that for $I_M = 10^{16}$ Wcm^{-2} the electron clouds are nearly spatially homogeneous with the majority of the electrons being located within the cluster (Fig. 6), while for $I_M = 10^{18}$ Wcm^{-2} the electron spatial distribution is inhomogeneous, assuming a "sausage type" structure along the laser electric field (Fig. 7). General characteristics of the nanoplasma are [7-9]:

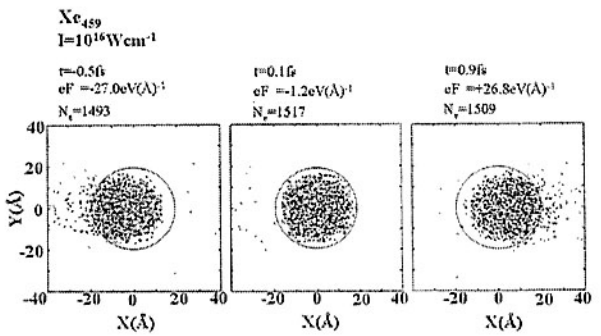

Fig. 6. The response of the electron cloud, which contains N_e electrons (black points) in the nanoplasma in a Xe_{459} cluster at $I_M = 10^{16}$ Wcm^{-2}. Circles represent the cluster size. Laser propagation direction along the X axis, with the electric field F_ℓ at time t.

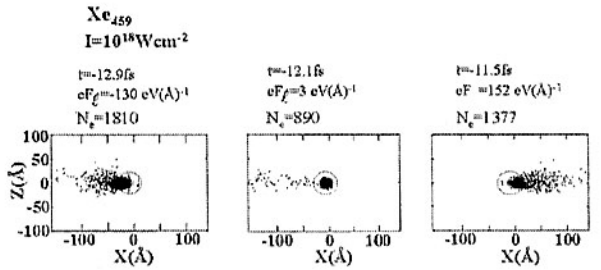

Fig. 7. Same as for Fig. 4 with $I_M = 10^{18}$ Wcm^{-2}.

(1) A "black cloud" of free electrons inside and in the vicinity of the cluster. (2) The nanoplasma is positively charged. (3) High average electron densities of ~(2-3)10^{22} cm^{-3}, being comparable to electron densities in metals. (4) High average electron energies of ~50eV-1keV, which increase with increasing I_M. (5) Spatial inhomogeneity and angular anisotropy induced by the laser field (Figs. 6 and 7). (6) The existence of a persistent nanoplasma with a lifetime τ_P > 100fs at $I_M = 10^{15}$-10^{16} Wcm^{-2}, and a transient nanoplasma with τ_P < 10fs at $I_M = 10^{18}$ Wcm^{-2} (Figs. 4 and 5). (7) Partial or complete depletion by outer ionization.

4. Energetics and Dynamics of Uniform and Nonuniform Coulomb Explosion

Cluster electron dynamics triggers nuclear dynamics, with the outer ionization being accompanied by CE [8-14,16,17]. The traditional view of CE involves a uniform explosion of a homonuclear cluster in the limit of cluster vertical ionization (CVI). The CVI time scales for multielectron ionization are short on the time scale of nuclear motion and outer ionization is complete [7-11]. We advanced [8,9] a border cluster radius $R_0^{(I)} \propto I_M^{1/2}$, with the CVI being applicable for $R_0 < R_0^{(I)}$. Under CVI conditions, the maximal ion energy for CE of $(A^{q_A+})_n$ is [8,9] $E_M = (4\pi/3)\bar{B}\rho_0 q_A^2 R_0^2$, the average ion energy is $E_{av} = (3/5)E_M$, while the distribution of the ion kinetic energies is $P(E) = (3/2E_M)(E/E_M)^{1/2}$ for $E \le E_M$, where ρ_0 is the constituent density and $\bar{B} = 14.40$eV. Uniform CE is well obeyed for elemental and homonuclear molecular clusters under sufficiently high I_M where the CVI conditions prevail. The average energies for CE of $(D_2)_{n/2}$ ($n = 459\text{-}3.3\cdot10^4$) clusters obey the CVI relation $E_{av} \propto R_0^2$ for $I_M > 10^{17}$ Wcm^{-2} (Fig. 8), while the energy distribution obeys the $P(E) \propto E^{1/2}$ relation (Fig. 9 and its left inset).

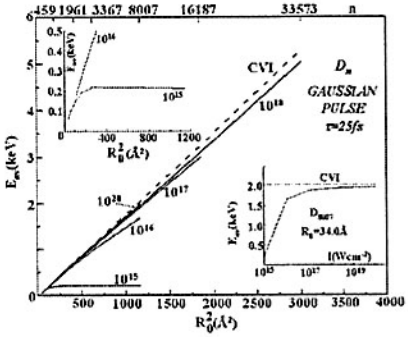

Fig. 8. Cluster size dependence of D^+ energies from CE of $(D_2)_{n/2}$ clusters (n = 354-33573) induced by Gaussian laser pulses with $I_M = 10^{15}$-10^{20}Wcm^{-2}, which are marked on the curves. The result of the CVI is also presented. The insets show severe deviations from the CVI at $I_M \le 10^{17}$ Wcm^{-2}.

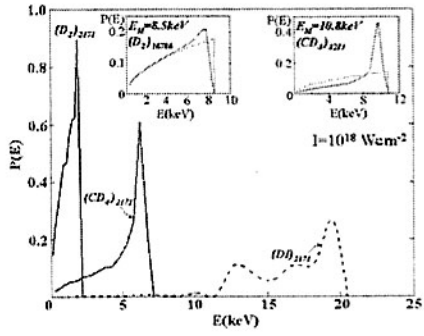

Fig. 9. Kinetic energy distribution P(E) of D^+ ions in the CE of $(D_2)_n$ and deuterium containing hetero-clusters at $I_M = 10^{18}$ Wcm^{-2}. The insets show the $P(E) \propto E^{1/2}$ CVI relation (dashed lines) and simulation results (solid lines).

The uniform CE picture breaks down for the explosion of $(A_k^{q_A+}B_\ell^{q_B+})_n$ heteroclusters consisting of A^{q_A+} ions of masss m_A and heavy $B_\ell^{q_B+}$ ions of mass m_B, e.g., $(H^+T^+)_n$, $(D_2^{++}O^{q+})$ (q = 6,8), $(C^{q+}D_4^{4+})_n$ (q = 4,6), $(D^+I^{q+})_n$ (q =

5-35), or $(C^{6+}D_3^{+3}I^{q+})_n$ (q = 5-35) heteroclusters [9,13,14]. Two major new effects in the CE of multicharged heteroclusters were predicted [9-14]:
(A) Energetic boosting of the energies of low-charged, light ions driven by the heavy ions. The energetics E_M and E_{av} of D^+ ions from the CE of $(D_2O)_n$, $(CD_4)_n$ or $(DI)_n$ clusters is expected to be considerably larger than for D^+ energies from $(D_2)_{n/2}$ clusters of the same size (Fig. 10).
(B) Kinematic driving effects, which are determined by the kinematic parameter $\eta_{AB} = q_A m_B / q_B m_A$. For $\eta_{AB} > 1$, a runover of the light ions over the heavy ions prevails, resulting in two distinct spatial distributions of the light/heavy ions [9,13,14]. At higher ion energies, the marked deviation of P(E) for CE of $(CD_4)_n$ heteroclusters (Fig. 9) is due to the runover effects. This process results in an isotope effect in the energetics of light ions from heterocluster CE (e.g., for $(CD_4)_n$ and for $(CH_4)_n$) [9], which was experimentally confirmed [19]. Extreme runover effects are manifested for CE of extremely charged light-heavy heteroclusters with large η_{AB} (e.g., $(H^+I^{25+})_n$ or $(D^+I^{25+})_n$), which reveal expanding, 2-dimentional spherical thin shells of light ions [13,14] (Fig. 11). The light ion energy distribution is narrow, falling in the vicinity of the high values of E_M (Fig. 9 for $(DI)_n$). These manifest the attainment of transient self-organization in complex systems driven by repulsive Coulomb interactions.

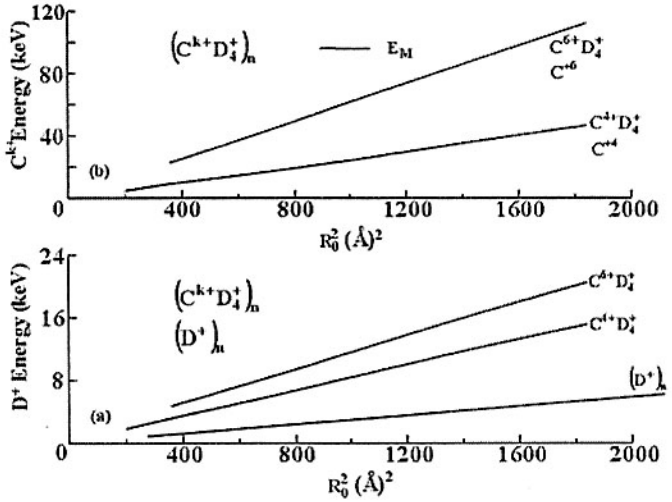

Fig. 10. Cluster size dependence of the maximal energy of ions in the CE of $(D_2)_n$ and $(CD_4)_n$, obeying the CVI relation. The marked D^+ energy boosting effects on the energy of D^+ ions in the CE of the heterocluster is manifested.

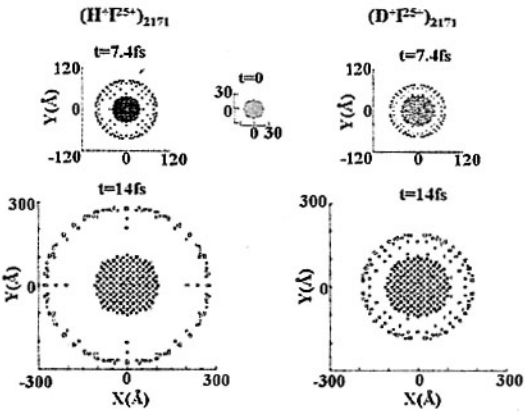

Fig. 11. 2-dimensional pictures of the time-dependent spatial configuration of ions in CE of $(H^+I^{25+})_{2171}$ and $(D^+I^{25+})_{2171}$ heteroclusters, which manifest extreme kinematic runover effects. (■) I^{25+} and (O) H^+ or D^+.

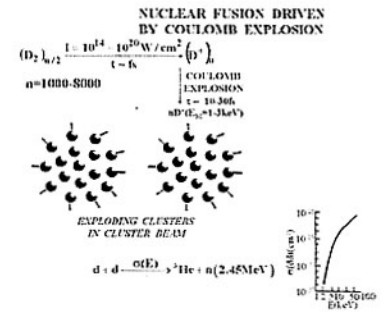

Fig. 12. Artist's view of NFDCE in an assembly of $(D_2)_n$ clusters, with energetic deuterons from different clusters undergoing dd fusion within the macroscopis plasma filament with the cross sections for dd fusion being represented in the lower part of the figure

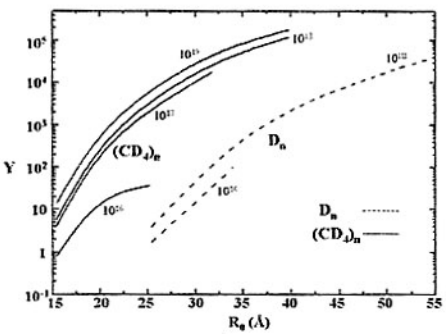

Fig. 13. Neutron yields pere laser pulse for dd NFDDCE of $(D_2)_n$ and $(CD_4)_n$ clusters (see text) at intensities $I_M = 10^{16}$-10^{18} Wcm^{-2} (marked in the curves).

5. Nuclear Fusion Driven by Cluster Coulomb Explosion

The energies of D^+ ions from CE of $(D_2)_{n/2}$ clusters in the range $E_M \leq 10$ keV (Fig. 8) fall in the domain of nuclear physics. Compelling experimental and theoretical evidence [2,4,9,20] was advanced for dd nuclear fusion driven by Coulomb explosion (NFDCE) in an assembly of deuterium $(D_2)_n$ clusters

(Fig. 12). We predicted [9-14,20] that the CE of highly charged heteronuclear deuterium containing molecular clusters will result in considerably higher D^+ energies due to energetics boosting effects (section 4 and Fig. 9 and 10) and a narrower energy distribution in the vicinity of E_M due to kinematic runover effects (section 4 and Fig. 9). The neutron yields Y (per laser pulse) calculated under the conditions of the Lawrence - Livermore experiment [2,4] for $I_M > 10^{17}$ Wcm^{-2} are higher by 2-3 orders of magnitude for CE of $(CD_4)_n$ clusters than for $(D_2)_n$ clusters of the same size (Fig. 13). These theoretical predictions [9-11] were experimentally confirmed in Sacley [3], the Lawrence-Livermore laboratory [4] and in the Max-Born Institute [21]. Moving to NFDCE of extremely charged light-heavy hetoercluster, e.g., $(D^+T^{25+})_n$ (Fig. 9), Y can be enhanced by another 2-3 orders of magnitude over $(CD_4)_n$ clusters of the same size. We are currently exploring further perspectives of nuclear reactions of astrophysical interest, e.g., in the CNO cycle in hot stars [22], which can be driven by table-top nucleosynthesis induced by heteroclusters CE.

During the last decade, cluster science explored new and fascinating territories, bridging between cluster electron-nuclear dynamics and table-top nuclear fusion.

Acknowledgement. This research was supported by the Deutsche Forschungsgemeinschaft (DFG) SFB 450 on "Analysis and Control of Ultrafast Photo-induced Reactions".

1. T. Ditmire et al. Phys. Rev. Lett. 78 (1997) 2832.
2. J. Zweiback et al. Phys. Rev. Lett. 84 (2000) 2634.
3. G. Gullon et. al. Phys. Rev. Lett. 89 (2002) 065005.
4. R.W. Madison et al. Phys. Plasmas 11 (2004) 270.
5. I. Last, J. Jortner, Phys. Rev. 64 (2001) 063201.
6. I. Last, J. Jortner, J. Chem. Phys. 120 (2004) 1336.
7. I. Last, J. Jortner, J. Chem. Phys. 120 (2004) 1348.
8. I. Last, J. Jortner, J. Chem. Phys. 121 (2004) 3030.
9. I. Last, J. Jortner, J. Chem. Phys. 121 (2004) 8329.
10. I. Last,J. Jortner, Phys. Rev. Lett. 87 (2001) 033401.
11. I. Last, J. Jortner, J. Phys. Chem. A 106 (2002) 10877.
12. J. Jortner, I. Last, ChemPhysChem 3 (2002) 845.
13. I. Last, J. Jortner, Proceed. Natl. Acad. Sci. USA 102 (2005) 1291.
14. I Last, J. Jortner, Phys. Rev. A 71 (2005) 063204.
15. C. Bréchignac et al. Phys. Rev. Lett. 64 (1990) 2893.
16. I. Last, Y. Levy, J. Jortner, J. Chem. Phys. 123 (2005) 154301.
17. O. Zhong, A.W. Castleman Jr., Chem. Rev. 100 (2000) 4039.
18. A. Heidenreich, I. Last, J. Jortner, Eur. Phys. J. D 35 (2005) 567.
19. M. Hohenberger et al. Phys. Rev. Lett. 95 (2005) 195003.
20. I. Last, J. Jortner, Phys. Rev. A 64 (2001) 063201.
21. S. Ter-Avetisyan ete al. Phys. Plas. 12 (2005) 12702.
22. G. Wallerstein et al. Rev. Mod. Phys. 69 (1997) 995